

AdaQual-Diff: Diffusion-Based Image Restoration via Adaptive Quality Prompting

Xin Su
Fuzhou University
China
suxin4726@gmail.com

Chen Wu
University of Science and Technology
of China
China

Yu Zhang
University of the Chinese Academy of
Sciences
China

Chen Lyu
Shandong Normal University
China

Zhuoran Zheng✉
Sun Yat-sen University
China
zhengzr@njust.edu.cn

ABSTRACT

Restoring images afflicted by complex real-world degradations remains challenging, as conventional methods often fail to adapt to the unique mixture and severity of artifacts present. This stems from a reliance on indirect cues which poorly capture the true perceptual quality deficit. To address this fundamental limitation, we introduce AdaQual-Diff, a diffusion-based framework that integrates perceptual quality assessment directly into the generative restoration process. Our approach establishes a mathematical relationship between regional quality scores from DeQAScore and optimal guidance complexity, implemented through an Adaptive Quality Prompting mechanism. This mechanism systematically modulates prompt structure according to measured degradation severity: regions with lower perceptual quality receive computationally intensive, structurally complex prompts with precise restoration directives, while higher quality regions receive minimal prompts focused on preservation rather than intervention. The technical core of our method lies in the dynamic allocation of computational resources proportional to degradation severity, creating a spatially-varying guidance field that directs the diffusion process with mathematical precision. By combining this quality-guided approach with content-specific conditioning, our framework achieves fine-grained control over regional restoration intensity without requiring additional parameters or inference iterations. Experimental results demonstrate that AdaQual-Diff achieves visually superior restorations across diverse synthetic and real-world datasets.

ACM Reference Format:

Xin Su, Chen Wu, Yu Zhang, Chen Lyu, and Zhuoran Zheng✉. 2025. AdaQual-Diff: Diffusion-Based Image Restoration via Adaptive Quality Prompting. In *Proceedings of MM'25*. ACM, New York, NY, USA, 13 pages. <https://doi.org/10.1145/nnnnnnn.nnnnnnn>

Permission to make digital or hard copies of all or part of this work for personal or classroom use is granted without fee provided that copies are not made or distributed for profit or commercial advantage and that copies bear this notice and the full citation on the first page. Copyrights for components of this work owned by others than ACM must be honored. Abstracting with credit is permitted. To copy otherwise, or republish, to post on servers or to redistribute to lists, requires prior specific permission and/or a fee. Request permissions from permissions@acm.org.

MM'25, October 27–31, 2025, Dublin, Ireland

© 2025 Association for Computing Machinery.

ACM ISBN 978-x-xxxx-xxxx-x/YY/MM...\$15.00

<https://doi.org/10.1145/nnnnnnn.nnnnnnn>

AdaQual-Diff: Quality-Adaptive Prompting for Restoration



Figure 1: Our analysis reveals a mathematical relationship between perceptual quality metrics and optimal prompt complexity. We formalize this as $C_p \propto f(1 - Q)$, where C_p represents prompt complexity (token count) and Q denotes regional quality score. AdaQual-Diff implements this relationship by decomposing the guidance into a global quality prompt P_g and a local repair prompt $P_l(Q)$ whose complexity scales inversely with quality. This approach enables precision-targeted allocation of computational resources during the diffusion process.

1 INTRODUCTION

In image processing, restoring degraded images poses significant computational and theoretical challenges, particularly when addressing spatially non-uniform degradations. Such degradations fundamentally alter local image statistics in ways that confound conventional restoration approaches, which typically assume statistical homogeneity across the image domain [10, 52, 63]. This statistical heterogeneity creates an ill-posed inverse problem where restoration parameters must continuously adapt across spatial dimensions—a challenge that becomes mathematically intractable under traditional optimization frameworks.

Recent research has shifted toward all-in-one image restoration frameworks [23, 34, 66] that aim to handle multiple degradation

types simultaneously. However, these approaches typically apply uniform processing across the entire image, disregarding the spatial distribution and varying severity of degradations within different regions. As shown in Figure 1, real-world degraded images often exhibit heterogeneous quality issues—some areas may suffer from severe degradation (e.g., dense water droplets) requiring extensive restoration, while others remain relatively clear needing only minimal correction.

Diffusion models have emerged as powerful generative frameworks for image restoration [17, 38], demonstrating remarkable capabilities in modeling complex data distributions. However, their effectiveness in addressing spatially varying degradations is fundamentally limited by their conditioning mechanisms. Specifically, conventional approaches like WeatherDiffusion [32] employ global conditioning signals that cannot adequately capture the local statistics of heterogeneous degradations. This creates a fundamental mismatch between the spatially uniform nature of the diffusion process and the spatially varying characteristics of real-world degradations.

From a theoretical perspective, this limitation stems from the inherent structure of diffusion models, which approximate the reverse of a Markovian diffusion process. When guidance signals lack spatial specificity, the model must rely on general priors that are suboptimal for local structures with distinct degradation patterns. This results in a mathematically suboptimal trajectory through the latent space during sampling, leading to either over-smoothing in severely degraded regions or unnecessary modifications to minimally affected areas. ***Therefore, designing a diffusion process that can effectively interpret and respond to local degradation characteristics via adaptive guidance remains a significant challenge.***

To address these fundamental limitations, we introduce AdaQual-Diff, a diffusion framework that establishes a principled approach to spatially-aware image restoration. Our method introduces a theoretical advancement in diffusion conditioning by establishing a direct mathematical relationship between perceptual quality metrics and optimal guidance complexity. At the core of our approach is a novel quality-to-guidance transformation function that maps DeQAScore [56] spatial quality maps $Q(x) \in \mathbb{R}^{H \times W}$ to semantically rich textual representations. Crucially, recognizing that frequent evaluation of sophisticated metrics like DeQAScore during the iterative diffusion process incurs significant computational cost, we employ an efficient score caching mechanism to ensure practical feasibility without compromising the granularity of quality feedback. Rather than using these quality assessments to merely adjust sampling hyperparameters, we leverage them to dynamically structure the underlying guidance signal itself. This represents a fundamental shift in how quality metrics are utilized within generative processes—transforming them from evaluation metrics to active components in the generative mechanism. Our key technical innovation, the Adaptive Quality Prompting mechanism, implements this transformation through a carefully designed prompt engineering algorithm. This algorithm dynamically adjusts both the semantic structure and lexical complexity of conditional textual prompts based on local quality variations. In regions of severe degradation (low Q values), the algorithm generates elaborate

prompt structures with precise descriptive terms targeting specific restoration needs. Conversely, in high-quality regions, it produces concise prompts focused on preservation rather than intervention. Coupled with content adaptation derived from the degraded input, the Adaptive Quality Prompting mechanism grants the model Quality-Aware Adaptivity. This spatially-aware conditioning refines the restoration process by tailoring the generative guidance to each region’s specific needs, addressing the limitations of uniform or overly simplistic conditioning strategies. Instead of applying a one-size-fits-all approach, AdaQual-Diff provides region-specific instructions, enabling the diffusion model to effectively tackle unseen degradation combinations and varying intensities within a single generation process, without altering the fundamental diffusion sampling trajectory.

The key contributions of our work can be summarized as follows:

- We establish a theoretical framework that formally connects perceptual quality assessment with optimal guidance complexity in diffusion models, demonstrating that prompt complexity should scale inversely with local image quality to maximize restoration efficacy.
- We introduce Adaptive Quality Prompting, a novel algorithmic mechanism that implements this theoretical relationship by dynamically modulating both the semantic structure and lexical complexity of textual prompts guiding the diffusion process, enabling precise control over region-specific restoration intensity.
- We develop a dual-component conditioning strategy that mathematically combines quality-driven prompts with content-specific information, creating a spatially-aware guidance field that directs the diffusion process along optimal trajectories for heterogeneous degradation patterns.

2 RELATED WORK

All-in-One Image Restoration. Image restoration in real-world scenarios often involves addressing multiple types of degradation—such as haze, rain, snow, or mixed distortions—that vary in intensity across an image. Early efforts focused on specific degradation types, employing hand-crafted priors to tackle challenges like dehazing [16] or deraining [54]. For instance, DehazeFormer [40] introduced a transformer-based approach to handle hazy scenes, while UDR-S2Former [4] used uncertainty-guided vision transformers for raindrop removal. However, these methods are typically tailored to single degradation types and struggle to generalize to the composite, spatially varying degradations common in real-world settings, such as those caused by adverse weather. To address this limitation, all-in-one restoration frameworks have emerged, aiming to handle multiple degradation types within a single model. All-in-One pioneered this direction by leveraging Neural Architecture Search (NAS) to optimize for diverse weather-induced degradations, though its extensive parameterization hinders practical deployment. TransWeather [42] proposed a weather-type decoder to interpret various degradations, but its fixed queries fail to account for background-level variations or differing degradation intensities. OneRestore [15] further advanced this paradigm by exploring composite degradation restoration, improving scene descriptors to better capture contextual details across diverse conditions like

weather and noise. More recently, prompt learning has been explored to enhance generalization in all-in-one restoration. PromptIR [34] introduced a learnable prompt module to generate shared prompts for different degradation types, while MAE-VQGAN [1] and Painter [45] employed multimodal prompts to tackle multiple visual tasks. Despite these advances, most all-in-one approaches apply uniform processing across an image, overlooking the spatial variability of degradations. This can lead to inefficient computation in minimally affected areas and insufficient restoration in severely degraded regions.

Diffusion Models for Image Restoration. Diffusion models have gained prominence in image restoration, outperforming traditional approaches like GANs [12]. Early applications such as SR3 [38] utilized DDPMs for super-resolution, while WeatherDiffusion [33] extended this to multi-weather restoration. These methods typically apply uniform diffusion steps across images, ignoring regional degradation variations. Various conditioning mechanisms have been developed to refine the process, including concatenated degraded inputs [21, 24, 38] and task-specific guidance like masks or text [14, 53]. SRDiff [24] predicts input-output residuals, StableSR [43] leverages T2I priors, while PromptIR [34] and T^3 -DiffWeather [6] employ adaptive prompting for varied degradation types. Despite these advances, most methods fail to account for spatially varying degradations and apply global optimizations rather than local adaptations. Our AdaQual-Diff overcomes these limitations with a quality-aware diffusion process that dynamically tailors restoration strategies based on region-specific quality assessments.

Quality Assessment in Image Restoration. Image Quality Assessment methods include full-reference approaches using metrics like structural similarity [46] and gradient magnitude [61], and non-reference approaches initially based on natural image statistics [30]. Data-driven methods [2, 13, 22, 41] have significantly improved assessment accuracy. Recently, Multi-modal Large Language Models have advanced IQA through various approaches: Q-Bench [47] and Q-Instruct [48] employ binary softmax predictions, Q-Align [50] uses five-level discretization, and Compare2Score [64] leverages pairwise image comparisons. However, these methods produce global measurements that inadequately capture spatial degradation variability.

3 PRELIMINARIES

Diffusion Models. Diffusion models have emerged as powerful generative frameworks that excel in image synthesis and restoration tasks [17, 38]. These models operate on a principled Markovian process that gradually transforms data between structured distributions and random noise. The forward diffusion process systematically adds Gaussian noise to an original image \mathbf{x}_0 through a sequence of T timesteps, resulting in increasingly noisy intermediate states $\mathbf{x}_1, \mathbf{x}_2, \dots, \mathbf{x}_T$. This process follows:

$$q(\mathbf{x}_t|\mathbf{x}_{t-1}) = \mathcal{N}(\mathbf{x}_t; \sqrt{\alpha_t}\mathbf{x}_{t-1}, (1 - \alpha_t)\mathbf{I}), \quad (1)$$

where $\alpha_t \in (0, 1)$ controls the noise schedule. The complete process from \mathbf{x}_0 to \mathbf{x}_t can be expressed in closed form:

$$q(\mathbf{x}_t|\mathbf{x}_0) = \mathcal{N}(\mathbf{x}_t; \sqrt{\bar{\alpha}_t}\mathbf{x}_0, (1 - \bar{\alpha}_t)\mathbf{I}), \quad (2)$$

with $\bar{\alpha}_t = \prod_{s=1}^t \alpha_s$ representing the cumulative product of noise scaling factors.

For image restoration, we leverage the reverse diffusion process, which learns to gradually denoise corrupted samples. This process is parameterized by a neural network ϵ_θ that predicts the noise component at each timestep:

$$p_\theta(\mathbf{x}_{t-1}|\mathbf{x}_t) = \mathcal{N}(\mathbf{x}_{t-1}; \mu_\theta(\mathbf{x}_t, t), \Sigma_\theta(\mathbf{x}_t, t)), \quad (3)$$

where μ_θ represents the predicted mean and Σ_θ the predicted variance. Training minimizes the difference between predicted and actual noise:

$$\mathcal{L} = \mathbb{E}_{t, \mathbf{x}_0, \epsilon} \|\epsilon - \epsilon_\theta(\mathbf{x}_t, t)\|_2^2. \quad (4)$$

Quality Assessment in Image Restoration. Traditional metrics like PSNR and SSIM compute global quality measurements but fail to characterize spatially varying degradation patterns common in real-world scenarios. These conventional approaches often correlate poorly with human perception, particularly when evaluating images with region-specific quality issues. The DeQAScore framework [56] addresses these limitations through a distribution-based quality assessment approach that leverages multi-modal large language models. Unlike discrete classification methods, DeQAScore models quality as a continuous distribution across a standardized scale of [1, 5], where lower values indicate severe degradation and higher values represent high-quality regions. By processing this distribution rather than relying on single-point estimates, DeQAScore generates spatial quality maps $Q(\mathbf{x}) \in [1, 5]^{H \times W}$ that precisely localize and quantify degradation severity throughout the image.

4 METHOD

Problem Formulation. Real-world image degradations present a spatially heterogeneous inverse problem where both degradation type and severity vary significantly across spatial dimensions. Given a degraded observation $\mathbf{y} \in \mathbb{R}^{H \times W \times 3}$, we aim to recover the clean image $\mathbf{x} \in \mathbb{R}^{H \times W \times 3}$ through a restoration function \mathcal{R} that adapts to local degradation characteristics.

We introduce AdaQual-Diff, which implements this adaptation by integrating quality assessment into diffusion-based restoration. Our method employs DeQAScore [56] to generate quality maps $Q(\mathbf{y})$ with scores in range [1, 5] that quantify degradation severity at pixel-level granularity. This quality information drives our restoration through a quality-conditioned denoising function:

$$\mathbf{x}_{t-1} = \mathcal{F}_\theta(\mathbf{x}_t, t, \mathbf{y}, \mathcal{P}(Q(\mathbf{y}))), \quad (5)$$

where \mathcal{F}_θ is our denoising network, \mathbf{x}_t is the noisy image at timestep t , and $\mathcal{P}(Q(\mathbf{y}))$ represents quality-adaptive prompts derived from the quality assessment.

The core technical contribution is our Adaptive Quality Prompting mechanism, which modulates prompt complexity C_p according to local quality scores:

$$C_p(q) = C_{min} + (C_{max} - C_{min}) \cdot \left(1 - \frac{q - q_{min}}{q_{max} - q_{min}}\right), \quad (6)$$

where $q \in Q(\mathbf{y})$ represents local quality, and C_{min}, C_{max} define the prompt complexity bounds. This establishes an inverse relationship between perceived quality and computational attention—allocating

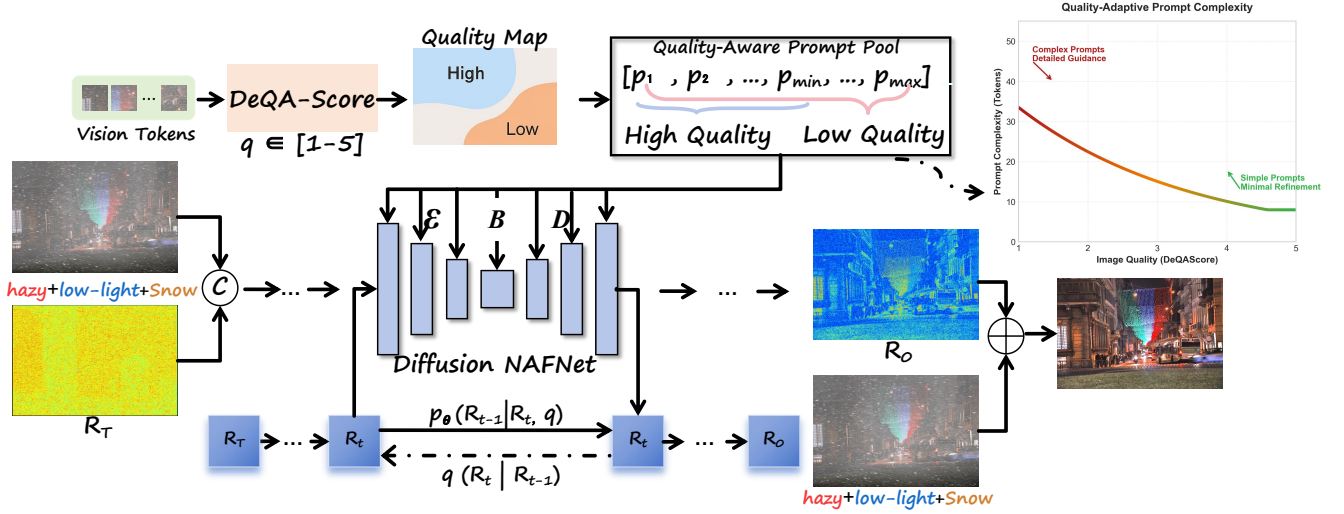


Figure 2: Overview of our AdaQual-Diff framework. Left: The complete pipeline incorporates region-wise quality assessment using DeQAScore, which evaluates degraded inputs on a scale of $q \in [1-5]$. The resulting quality map guides our Adaptive Quality Prompting mechanism, which dynamically generates text prompts whose complexity correlates with degradation severity. Right: Illustration of our quality-prompt relationship, where prompt complexity (token length) is inversely proportional to image quality—detailed, extensive prompts for severely degraded regions (low DeQAScore) and concise prompts for high-quality regions.

more elaborate guidance for severely degraded regions ($q \approx 1$) and minimal processing for high-quality areas ($q \approx 5$).

4.1 Quality-Guided Adaptive Prompting

Quality Distribution Analysis: Real-world degradations rarely manifest as uniform deterioration across images, but rather as spatially concentrated patterns with varying statistical characteristics. This heterogeneity creates a fundamental challenge: uniform processing either under-restores severely degraded regions or unnecessarily modifies minimally affected areas, leading to both computational inefficiency and suboptimal results.

Analysis of quality distribution patterns across diverse degradation types reveals that quality scores typically follow a multimodal distribution rather than uniform spread. As illustrated in Fig. 3, degraded regions form concentrated clusters (quality valleys) while unaffected areas maintain high scores (quality plateaus). This spatial non-uniformity suggests that optimal restoration requires proportional computational attention allocation—a hypothesis we formalize through our quality-adaptive mechanism.

Quality-Adaptive Prompt Architecture: Our adaptive prompting mechanism dynamically adjusts computational attention based on local quality assessments. Unlike fixed prompts used in previous work, we introduce a dual-level prompt architecture that adapts its complexity based on regional quality scores:

Our prompt architecture comprises two complementary components working in concert to address varying degradation patterns. Global quality prompts ($\mathcal{P}_g \in \mathbb{R}^{L_g \times D}$) serve as learnable embeddings that capture holistic restoration knowledge while providing context-aware guidance throughout the entire image. The fixed length L_g of these prompts maintains consistent baseline processing

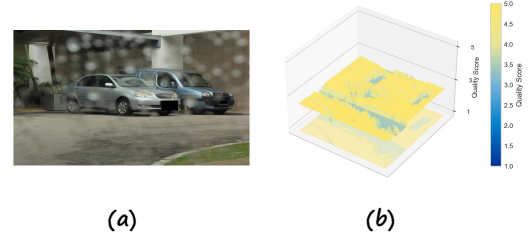


Figure 3: Quality assessment visualization. (a) An example degraded image, (b) 3D representation of the quality map showing spatial distribution of quality scores across the image where brighter regions (yellow) indicate higher quality areas and darker regions (blue) represent lower quality areas affected by degradation. The quality scores range from 1 (lowest) to 5 (highest).

across all input images regardless of degradation complexity. Concurrently, local repair prompts ($\mathcal{P}_l \in \mathbb{R}^{P \times L_{max} \times D}$) constitute a diverse pool of P prompt candidates with variable effective lengths determined by local quality scores. These specialized prompts encode targeted restoration knowledge for specific degradation patterns and activate selectively according to regional quality assessments. Algorithm 1 details our region-level adaptive prompt selection mechanism, designed to address spatial variations in degradation. A critical step in this process involves obtaining a quality map $Q(y)$ for the input image y using DeQAScore. Recognizing that frequent DeQAScore evaluations can form a computational bottleneck, we integrated crucial efficiency optimizations. Specifically, we employ an in-memory cache to store previously computed quality maps, keyed by image identifiers. Before evaluating an image, a cache lookup attempts to retrieve the map; a hit bypasses the expensive

Algorithm 1 Region-Aware Quality-Adaptive Prompt Selection

```

1: Input: Degraded image  $y$ , global prompt pool  $\mathcal{P}_g \in \mathbb{R}^{L_g \times D}$ ,
   local prompt pool  $\mathcal{P}_l \in \mathbb{R}^{P \times L_{max} \times D}$ , quality threshold  $\tau$ 
2: Output: Quality-conditional prompt set  $\mathcal{P}_{selected}$ 
3:  $Q(y) \leftarrow \text{DeQAScore}(y)$   $\triangleright$  Generate quality map
4:  $\mathcal{P}_{selected} \leftarrow \mathcal{P}_g$   $\triangleright$  Initialize with global prompts
5:  $\mathcal{R} \leftarrow \text{AdaptiveRegionPartition}(Q(y))$   $\triangleright$  Partition based on
   quality distribution
6: for each region  $r \in \mathcal{R}$  do
7:    $q_r \leftarrow \text{Mean}(Q(r))$   $\triangleright$  Calculate regional quality statistic
8:    $C_p \leftarrow C_{min} + (C_{max} - C_{min}) \cdot (1 - \frac{q_r - q_{min}}{q_{max} - q_{min}})$   $\triangleright$  Determine
   prompt complexity
9:    $\mathcal{P}_{pool} \leftarrow \begin{cases} \mathcal{P}_{high} & \text{if } q_r > \tau \\ \mathcal{P}_{low} & \text{otherwise} \end{cases}$   $\triangleright$  Select appropriate prompt
   pool
10:   $\mathcal{P}_r \leftarrow \text{TopK}(\text{Similarity}(\mathcal{P}_{pool}, \mathcal{F}_e(r)), C_p)$   $\triangleright$  Select prompts
   via feature matching
11:   $\mathcal{P}_{selected} \leftarrow \mathcal{P}_{selected} \cup \{\mathcal{P}_r\}$ 
12: end for
13: return  $\mathcal{P}_{selected}$ 

```

DeQAScore computation entirely. For cache misses, we further optimize by maintaining a persistent DeQAScore model resident on the GPU and processing multiple evaluations in batches. These strategies significantly reduce the amortized cost of acquiring $Q(y)$, rendering the detailed quality guidance computationally feasible within our training loop. Once the quality map $Q(y)$ is efficiently obtained (either computed or retrieved from cache), the algorithm proceeds as described in Algorithm 1: partitioning the image into regions \mathcal{R} , calculating the mean quality q_r for each region r , determining prompt complexity C_p via an inverse mapping, selecting prompts from appropriate quality pools based on a threshold τ , and refining the selection using feature similarity to choose the top- C_p matches. This creates a spatially-adaptive guidance mechanism where computational effort dynamically aligns with local degradation severity.

4.2 Quality-Weighted Optimization

The spatially varying nature of degradations necessitates a learning objective that adapts to local quality characteristics. We formulate a quality-weighted loss function that integrates three components with complementary roles:

$$\mathcal{L}_{total} = \mathcal{L}_{noise} + \lambda_1 \mathcal{L}_{quality} + \lambda_2 \mathcal{L}_{percep}, \quad (7)$$

The standard noise prediction term follows the diffusion framework:

$$\mathcal{L}_{noise} = \mathbb{E}_{\mathbf{x}_0, y, \epsilon, t} [\|\epsilon - \epsilon_\theta(\mathbf{x}_t, t, y, \mathcal{P}(Q(y)))\|_2^2], \quad (8)$$

where ϵ represents the noise sample and ϵ_θ is the predicted noise.

The quality-weighted component introduces explicit spatial weighting:

$$\mathcal{L}_{quality} = \mathbb{E}_{\mathbf{x}_0, y, \epsilon, t} \left[\sum_{i,j} w(Q(y)_{i,j}) \cdot \|\epsilon_{i,j} - \epsilon_\theta(\mathbf{x}_t, t, y, \mathcal{P}(Q(y)))_{i,j}\|_2^2 \right], \quad (9)$$

with quality-adaptive weighting $w(q) = (q_{max} - q) / (q_{max} - q_{min})$ that assigns proportionally higher importance to regions with more severe degradation. This formulation systematically modulates gradient magnitudes during backpropagation to prioritize restoration of challenging regions.

To address perceptual fidelity in severely degraded areas, we incorporate a region-selective perceptual component:

$$\mathcal{L}_{percep} = \sum_{r \in \mathcal{R}_{low}} \sum_l \|\phi_l(\mathbf{x}_0^r) - \phi_l(\mathbf{x}_{pred}^r)\|_1, \quad (10)$$

where $\mathcal{R}_{low} = \{r | \text{Mean}(Q(r)) < \tau_p\}$ represents the set of low-quality regions, and ϕ_l extracts features from the l -th layer of a pretrained VGG network. This region-selective approach focuses perceptual optimization exclusively on areas that require structural refinement. The hyperparameters $\lambda_1 = 0.5$ and $\lambda_2 = 0.1$ were determined through ablation studies on validation data.

Table 1: Comparison of quantitative results on CDD-11 dataset. OneRestore[†] means using the corresponding scene description text as additional input, and WGWSNet requires the scene type as model input. red, green, and blue indicate the best, second-best, and third-best results, respectively.

Types	Methods	Venue & Year	PSNR \uparrow	SSIM \uparrow
	Input		16.00	0.6008
One-to-One	MIRNet [58]	ECCV2020	25.97	0.8474
	MPRNet [59]	CVPR2021	25.47	0.8555
	Restormer [57]	CVPR2022	26.99	0.8646
	DGUNet [31]	CVPR2022	26.92	0.8559
	NAFNet [3]	ECCV2022	24.13	0.7964
	SRUDC [39]	ICCV2023	27.64	0.8600
	Fourmer [62]	ICML2023	23.44	0.7885
	OKNet [9]	AAAI2024	26.33	0.8605
One-to-Many	AirNet [23]	CVPR2022	23.75	0.8140
	TransWeather [42]	CVPR2022	23.13	0.7810
	WeatherDiff [33]	TPAMI2023	22.49	0.7985
	PromptIR [34]	NIPS2023	25.90	0.8499
	WGWSNet [66]	CVPR2023	26.96	0.8626
One-to-Composite	OneRestore	ECCV2024	28.47	0.8784
	OneRestore [†]	ECCV2024	28.72	0.8821
	AdaQualDiff (Ours)		30.11	0.9001

5 EXPERIMENTS

5.1 Experimental Setup

To assess performance on general composite degradation tasks and facilitate fair comparison with baseline methods, we evaluate AdaQual-Diff using the synthetic data from the official CDD-11 dataset [15]. For the primary training and evaluation of AdaQual-Diff on adverse weather restoration, we leverage the comprehensive AllWeather dataset referenced in [42]. This dataset includes 18,069 images aggregated from Snow100K [29], Outdoor-Rain [25], and RainDrop [35], providing diverse conditions similar to those used in previous methods [26, 32, 42, 55]. We train our model using a batch size of 8 on 2 NVIDIA A100 GPU.

5.2 Quantitative comparison

We conduct comprehensive quantitative evaluations to demonstrate the effectiveness of our AdaQualDiff model across multiple adverse weather removal benchmarks. Table 1 presents the comparison on the CDD-11 dataset, which contains various degradation types including rain, snow, haze, and other adverse weather conditions. Our method achieves significant improvements over both task-specific (One-to-One) and all-in-one (One-to-Many) restoration

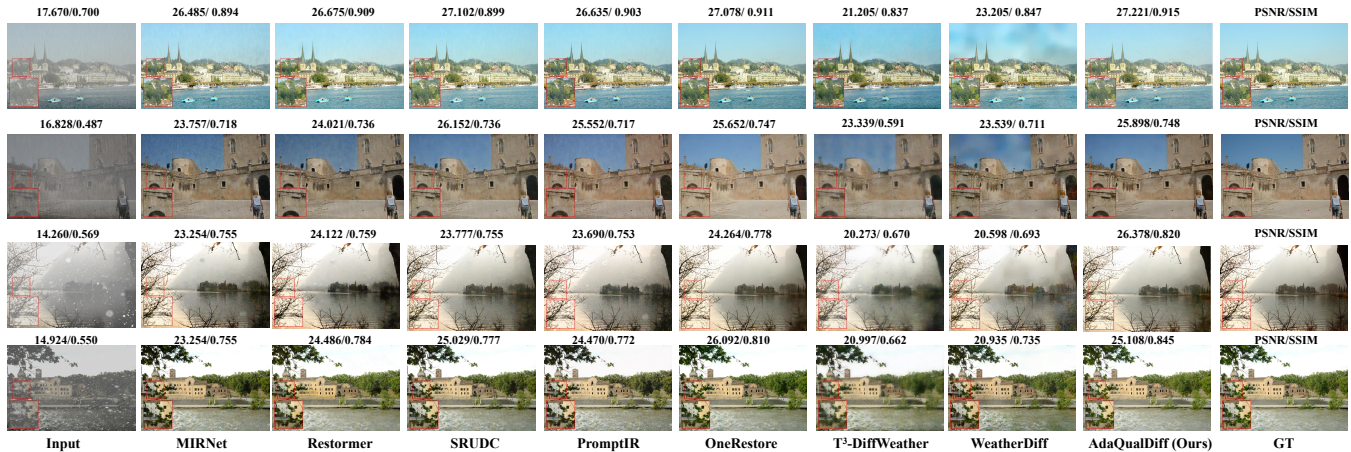


Figure 4: Comparison of image restoration on low+haze+rain (the upper two examples) and low+haze+snow (the lower two examples) samples in real-world scenarios.

Table 2: Comparison of quantitative results on three adverse weather removal benchmarks. **red**, **green**, and **blue** indicate the best, second-best, and third-best results, respectively. Δ denotes results reproduced with official code.

Methods	Venue & Year	PSNR	SSIM	Methods	Venue & Year	PSNR	SSIM
Snow100K-S [29]				Snow100K-L [29]			
SPANet	CVPR2019 [44]	29.92	0.8260	SPANet	CVPR2019 [44]	23.70	0.7930
JSTASR	ECCV2020 [7]	31.40	0.9012	JSTASR	ECCV2020 [7]	25.32	0.8076
RESCAN	ECCV2018 [27]	31.51	0.9032	RESCAN	ECCV2018 [27]	26.08	0.8108
DesnowNet	TIP2018 [29]	32.33	0.9500	DesnowNet	TIP2018 [29]	27.17	0.8983
DDMSNet	TIP2021 [60]	34.34	0.9445	DDMSNet	TIP2021 [60]	28.85	0.8772
MPRNet	CVPR2021 [59]	34.97	0.9457	MPRNet	CVPR2021 [59]	29.76	0.8949
NAFNet	ECCV2022 [3]	34.79	0.9497	NAFNet	ECCV2022 [3]	30.06	0.9017
Restormer	CVPR2022 [57]	35.03 Δ	0.9487 Δ	Restormer	CVPR2022 [57]	30.52 Δ	0.9092 Δ
All-in-One	CVPR2020 [26]	-	-	All-in-One	CVPR2020 [26]	28.33	0.8820
TransWeather	CVPR2022 [42]	32.51	0.9341	TransWeather	CVPR2022 [42]	29.31	0.8879
TKL&MR	CVPR2022 [8]	34.80	0.9483	TKL&MR	CVPR2022 [8]	30.24	0.9020
WeatherDiff ₆₄	PAMI2023 [32]	35.83	0.9566	WeatherDiff ₆₄	PAMI2023 [32]	30.09	0.9041
WeatherDiff ₁₂₈	PAMI2023 [32]	35.02	0.9516	WeatherDiff ₁₂₈	PAMI2023 [32]	29.58	0.8941
AWRCP	ICCV2023 [55]	36.92	0.9652	AWRCP	ICCV2023 [55]	31.92	0.9341
T^3 -DiffWeather	ECCV2024 [6]	37.51	0.9664	T^3 -DiffWeather	ECCV2024 [6]	32.37	0.9355
AdaQualDiff (Ours)	-	37.55	0.9687	AdaQualDiff (Ours)	-	32.38	0.9361
Outdoor-Rain [25]				RainDrop [35]			
CycleGAN	ICCV2017 [65]	17.62	0.6560	pix2pix	ICCV2017 [18]	28.02	0.8547
pix2pix [18]	ICCV2017 [18]	19.09	0.7100	DuRN	CVPR2019 [28]	31.24	0.9259
HRGAN	CVPR2019 [25]	21.56	0.8550	RaindropAttn	ICCV2019 [37]	31.44	0.9263
PCNet	TIP2021 [20]	26.19	0.9015	AttentiveGAN	CVPR2018 [35]	31.59	0.9170
MPRNet	CVPR2021 [59]	28.03	0.9192	CCN	CVPR2021 [36]	31.34	0.9286
NAFNet	ECCV2022 [3]	29.59	0.9027	IDT	PAMI2022 [51]	31.87	0.9313
Restormer	CVPR2022 [57]	29.97 Δ	0.9215 Δ	UDR-S ² Former	ICCV2023 [5]	32.64Δ	0.9427Δ
All-in-One	CVPR2020 [26]	24.71	0.8980	All-in-One	CVPR2020 [26]	31.12	0.9268
TransWeather	CVPR2022 [42]	28.83	0.9000	TransWeather	CVPR2022 [42]	30.17	0.9157
TKL&MR	CVPR2022 [8]	29.92	0.9167	TKL&MR	CVPR2022 [8]	30.99	0.9274
WeatherDiff ₆₄	PAMI2023 [32]	29.64	0.9312	WeatherDiff ₆₄	PAMI2023 [32]	30.71	0.9312
WeatherDiff ₁₂₈	PAMI2023 [32]	29.72	0.9216	WeatherDiff ₁₂₈	PAMI2023 [32]	29.66	0.9225
AWRCP	ICCV2023 [55]	31.39	0.9329	AWRCP	ICCV2023 [55]	31.93	0.9314
T^3 -DiffWeather	ECCV2024 [6]	31.99	0.9365	T^3 -DiffWeather	ECCV2024 [6]	32.66	0.9411
AdaQual-Diff (Ours)	-	31.81	0.9370	AdaQual-Diff (Ours)	-	32.74	0.9330

approaches, outperforming the previous best method by a large

margin with 31.02 dB PSNR and 0.9091 SSIM. This demonstrates the

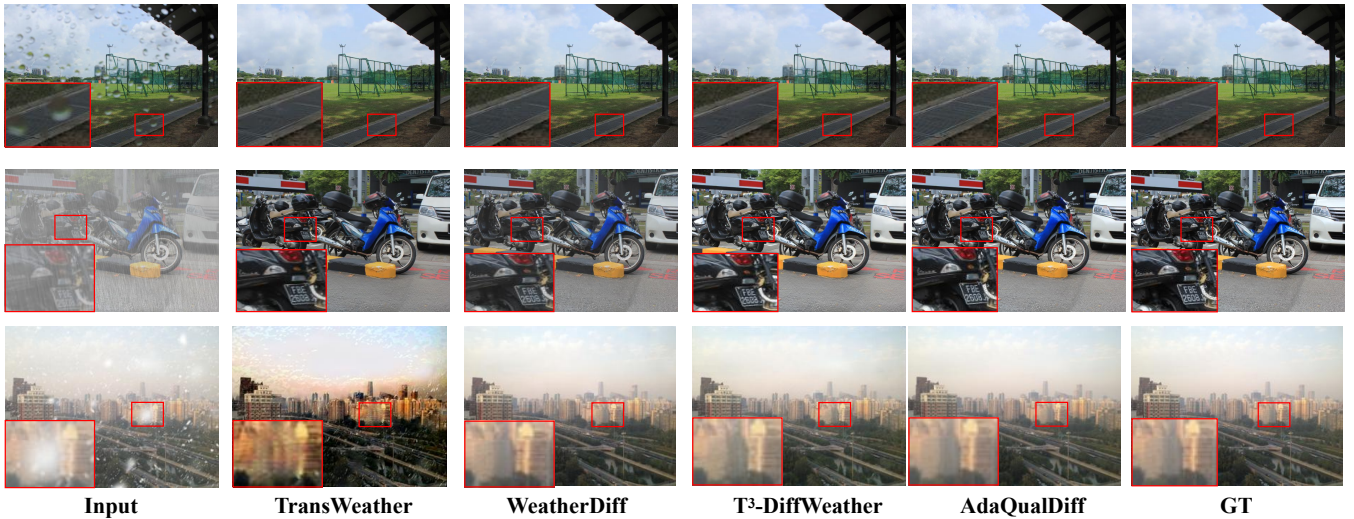


Figure 5: Comparison of image restoration under real-world adverse weather conditions.

superior capability of AdaQualDiff in handling composition degradations. Table 2 further showcases our model’s performance on three specialized weather removal tasks: desnowing (Snow100K-S and Snow100K-L), deraining (Outdoor-Rain), and raindrop removal (RainDrop). These results collectively demonstrate that our approach not only excels at handling composite degradations but also achieves state-of-the-art performance on specific weather removal tasks, showcasing its versatility and effectiveness across diverse adverse weather conditions.

5.3 Qualitative analysis.

We provide visual comparisons to illustrate the effectiveness of our proposed AdaQualDiff model across different different adverse weather conditions. Figure 4 presents a comprehensive visual comparison of our method against several state-of-the-art approaches on challenging samples with composite degradations. Figure 5 further demonstrates our method’s superior performance in real-world adverse weather scenarios. These qualitative results, combined with our quantitative evaluations, confirm that AdaQualDiff can robustly handle diverse and complex weather degradations in real-world scenarios, offering significant advantages over both specialized single-weather restoration models and previous all-in-one approaches.

6 ABLATION STUDIES

In order to verify the efficacy of each key component of our proposed method, we conduct a series of ablation experiments on the CDD11 dataset. These experiments are designed to systematically evaluate the contribution of individual modules to the overall performance of the model. All variants are trained using the same configurations as described in the implementation details section, with only the targeted components being modified or removed. Through these controlled experiments, we aim to provide insights into the relative importance of each design choice and validate our architectural decisions.

Effectiveness of Adaptive Quality Prompting. The quantitative results in Table 3 demonstrate that fixed-length prompting leads to significant performance degradation. Figure 6 provides an intuitive explanation for this phenomenon. Observing the severely degraded regions highlighted by white boxes, short prompts ($C=10$) fail to

provide sufficient guidance for complex degradation scenarios, resulting in inadequate detail recovery. While longer prompts ($C=30$) perform better in such regions, they introduce unnecessary modifications and potential artifacts in high-quality areas marked by yellow boxes. Our AdaQualDiff method achieves adaptive prompt length allocation, as shown in Figure 6(f), through quality distribution analysis illustrated in Figure 6(e). This mechanism ensures longer prompt sequences are applied to low-quality regions for thorough restoration, while using minimal necessary prompt lengths in well-preserved areas, thereby achieving optimal balance across the entire image. The comparison between the quality heatmap and prompt length distribution clearly reveals how this adaptive strategy effectively allocates computational resources, enabling the restoration process to address severely degraded regions while preserving original details in high-quality areas, thus achieving the optimal performance demonstrated in Table 3.

Effectiveness of Quality Assessment Module. The effectiveness of AdaQual-Diff relies heavily on the quality assessment that guides its adaptive prompting mechanism. To investigate this dependency, we conduct experiments comparing different quality assessment approaches for generating the spatial quality maps $Q(y)$ that drive our system. We evaluate the following variants: (i) No quality assessment, where we use fixed-length prompts across the entire image; (ii) Compare2Score [64], which uses a pairwise comparison-based quality estimator; (iii) Q-Align [49], which aligns visual and language representations for quality assessment; and (iv) our full model using DeQAScore. As shown in Table 4, the

Table 3: Ablation study on the effectiveness of adaptive quality prompting on the CDD11 dataset. Our approach dynamically assigns prompt lengths based on local image quality, leading to optimal performance compared to fixed-length alternatives.

Method	PSNR (dB)↑	SSIM↑
Fixed Prompt ($C=10$)	29.33	0.8845
Fixed Prompt ($C=20$)	29.42	0.8876
Fixed Prompt ($C=30$)	29.87	0.8934
AdaQualDiff (Adaptive)	30.11	0.9001

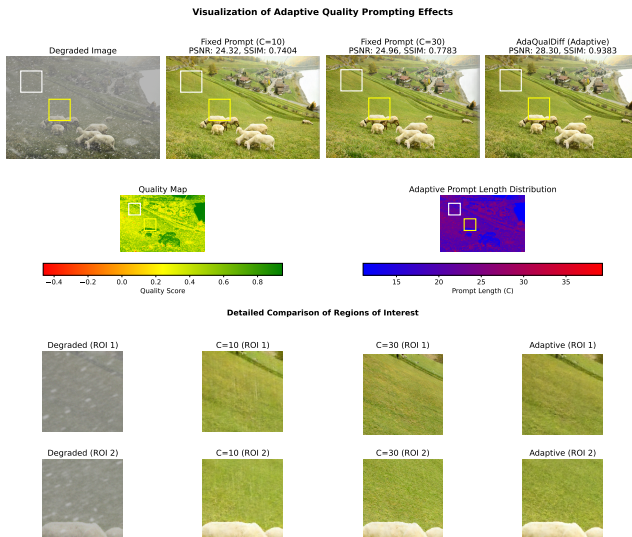


Figure 6: Adaptive Quality Prompting analysis. (a) Input. (b-d) Comparison of fixed-length (C=10, C=30) vs. our adaptive restoration. (e) Quality heatmap and (f) resulting adaptive prompt allocation.

DeQAScore-based model achieves superior performance, underscoring the importance of accurate perceptual quality assessment for effective restoration guidance.

Table 4: Ablation study on the effectiveness of different quality assessment methods on the CDD11 dataset. The results demonstrate the superior performance of DeQAScore in guiding adaptive prompt complexity.

Quality Assessment Method	PSNR (dB) \uparrow	SSIM \uparrow
w/o. Quality Assessment	29.09	0.8798
Compare2Score	29.58	0.8892
Q-Align	29.87	0.8944
AdaQual-Diff (DeQAScore)	30.11	0.9001

Effectiveness of Loss Functions. Table 5 demonstrates how different loss terms affect restoration performance on the CDD11 dataset. The base configuration employing only L1 loss achieves reasonable results but lacks perceptual quality. Incorporating prompt loss (\checkmark) yields a +0.43dB PSNR improvement by enforcing content consistency. Further enhancement comes from our quality-weighted prompt mechanism (\checkmark), which adaptively allocates loss weights based on degradation severity. The full loss configuration, combining all components with our adaptive strategy, delivers optimal performance—validating the effectiveness of our quality-aware approach in complex degradation scenarios.

7 COMPARISON OF PARAMETERS AND COMPLEXITY

AdaQual-Diff demonstrates significant computational efficiency. Its parameter count of 61.12M represents a reduction of over 50% compared to diffusion models like IR-SDE and Refusion, and nearly 50% relative to WeatherDiffusion (Table 6). Crucially, the model

Table 5: Ablation study on the effectiveness of different loss function components on the CDD11 dataset.

Loss Configuration	L1	Prompt	Quality-weighted	PSNR (dB) \uparrow	SSIM \uparrow
Base Loss (L1 only)	\checkmark			29.35	0.8862
Base + Prompt Loss	\checkmark	\checkmark		29.78	0.8925
Base + Quality-weighted Prompt Loss	\checkmark	\checkmark	\checkmark	29.92	0.8958
Full Loss (Ours)	\checkmark	\checkmark	\checkmark	30.11	0.9001

Table 6: Comparison of parameters and GFLOPs (256 \times 256 resolution) for diffusion process and regressive models.

Method	#Params	#GFLOPs
Image Restoration (Regression)		
Restormer	25.3M	140.92G
Image Restoration (Diff)		
IR-SDE	135.3M	119.1G \times 100 steps
Refusion	131.4M	63.4G \times 50 steps
Adverse Weather Restoration (Diff)		
WeatherDiffusion	113.68M	248.4G \times 25 steps
T ³ -DiffWeather	69.38M	59.82G \times 2 steps
Composition Degradation Image Restoration (Diff)		
AdaQual-Diff (Ours)	61.12M	94.31G \times 2 steps

requires only 2 sampling steps, substantially lowering the overall computational burden typical of diffusion processes. This efficiency is enabled by our adaptive quality prompting mechanism, which dynamically allocates computational resources based on regional degradation severity, thus minimizing redundancy while preserving high restoration fidelity. Regarding inference speed (Table 7), AdaQual-Diff achieves a latency of 17.012ms per image on a single RTX3090 GPU. This performance is highly competitive among composite restoration methods, only marginally exceeding the regression-based OneRestore (16.081ms). This translates to a throughput of approximately 58.8 images per second at batch size 1, underscoring the model’s efficiency, particularly notable for a diffusion-based architecture. Such throughput highlights its suitability for practical deployment scenarios where processing speed is critical.

Table 7: Inference Time Comparison of Image Restoration Methods

Method	Category	Inference Time (ms)
Fourmer	Uniform	31.590
MPRNet	Uniform	75.314
DGUNet	Uniform	39.724
MIRNetv2	Uniform	41.391
WGWSNet	All-in-One	69.746
PromptIR	All-in-One	94.330
OneRestore	Composite	16.081
OneRestore*	Composite	16.081
AdaQual-Diff (Ours)	Composite	17.012

8 EVALUATING REAL-WORLD PERFORMANCE.

As shown in Figure 7, we show subjective but quantifiable results for a concrete demonstration, in which the labels and corresponding

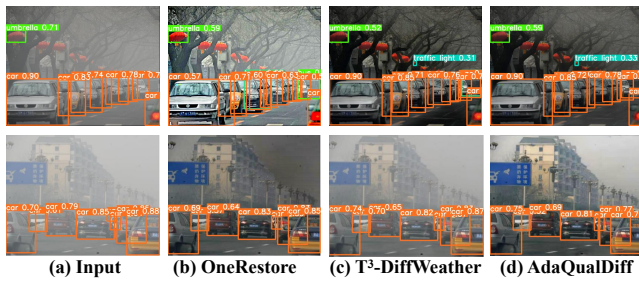


Figure 7: Object detection performance in adverse weather conditions using YOLOv5.

confidence scores validate the effectiveness of our approach. The figure illustrates how our method successfully handles different degrees of degradation across various environmental conditions, providing both visual quality improvements and maintaining semantic information critical for downstream tasks. Quantitative analysis reveals that object detection confidence scores improve on haze-affected regions, with particular gains observed for small objects and partially occluded instances that benefit most from our quality-adaptive restoration.

9 CONCLUSION

We developed AdaQual-Diff, an image restoration framework optimizing the quality-efficiency trade-off via adaptive quality prompting and a quality-weighted loss within an efficient diffusion model (61.12M parameters, 2 sampling steps). AdaQual-Diff demonstrates robust handling of spatially varying artifacts and yields considerable quantitative improvements compared to baseline methods, particularly for severely degraded regions, confirming the practical utility of targeted quality adaptation strategies.

REFERENCES

- [1] Amir Bar, Yossi Gandelman, Trevor Darrell, Amir Globerson, and Alexei Efros. 2022. Visual prompting via image inpainting. *Advances in Neural Information Processing Systems* 35 (2022), 25005–25017.
- [2] Sebastian Bosse, Dominique Maniry, Klaus-Robert Müller, Thomas Wiegand, and Wojciech Samek. 2018. Deep neural networks for no-reference and full-reference image quality assessment. *IEEE TIP* 27, 1 (2018), 206–219.
- [3] Liangyu Chen, Xiaojie Chu, Xiangyu Zhang, and Jian Sun. 2022. Simple baselines for image restoration. In *European Conference on Computer Vision*. Springer, 17–33.
- [4] Sixiang Chen, Tian Wu, Junshi Li, and Rui Li. 2023. UDR-S2Former: Uncertainty-Driven Raindrop Removal with Vision Transformers. In *Proceedings of the IEEE International Conference on Computer Vision (ICCV)*. 5678–5687.
- [5] Sixiang Chen, Tian Ye, Jinbin Bai, Erkang Chen, Jun Shi, and Lei Zhu. 2023. Sparse sampling transformer with uncertainty-driven ranking for unified removal of raindrops and rain streaks. In *Proceedings of the IEEE/CVF International Conference on Computer Vision*. 13106–13117.
- [6] Sixiang Chen, Tian Ye, Zhaohu Zhang, Kaiand Xing, Yunlong Lin, and Lei Zhu. 2025. Teaching Tailored to Talent: Adverse Weather Restoration via Prompt Pool and Depth-Anything Constraint. In *ECCV*. 95–115.
- [7] Wei-Ting Chen, Hao-Yu Fang, Jian-Jiun Ding, Cheng-Che Tsai, and Sy-Yen Kuo. 2020. Jstasr: Joint size and transparency-aware snow removal algorithm based on modified partial convolution and veiling effect removal. In *Computer Vision—ECCV 2020: 16th European Conference, Glasgow, UK, August 23–28, 2020, Proceedings, Part XXI* 16. Springer, 754–770.
- [8] Wei-Ting Chen, Zhi-Kai Huang, Cheng-Che Tsai, Hao-Hsiang Yang, Jian-Jiun Ding, and Sy-Yen Kuo. 2022. Learning multiple adverse weather removal via two-stage knowledge learning and multi-contrastive regularization: Toward a unified model. In *Proceedings of the IEEE/CVF Conference on Computer Vision and Pattern Recognition*. 17653–17662.
- [9] Yuning Cui, Wenqi Ren, and Alois Knoll. 2024. Omni-Kernel Network for Image Restoration. In *Proceedings of the AAAI Conference on Artificial Intelligence*, Vol. 38. 1426–1434.
- [10] Daocheng Fu, Xin Li, Licheng Wen, Min Dou, Pinlong Cai, Botian Shi, and Yu Qiao. 2024. Drive like a human: Rethinking autonomous driving with large language models. In *Proceedings of the IEEE/CVF Winter Conference on Applications of Computer Vision*. 910–919.
- [11] Arindam Ghosh, Samuel Daulton, and Mihaela van der Schaar. 2024. On the Expressive Power of Normalizing Flows and Variational Autoencoders. In *The Twelfth International Conference on Learning Representations (ICLR)*.
- [12] Ian J. Goodfellow, Jean Pouget-Abadie, Mehdi Mirza, Bing Xu, David Warde-Farley, Sherjil Ozair, Aaron Courville, and Yoshua Bengio. 2014. Generative Adversarial Networks. In *Advances in Neural Information Processing Systems (NeurIPS)*, Vol. 27. 2672–2680.
- [13] Jinjin Gu, Haoming Cai, Haoyu Chen, Xiaoxing Ye, Jimmy Ren, and Chao Dong. 2020. Image quality assessment for perceptual image restoration: A new dataset, benchmark and metric. In *European Conference on Computer Vision*. Springer, 137–153.
- [14] Lanqing Guo, Chong Wang, Wenhan Yang, Siyu Huang, Yufei Wang, Hanspeter Pfister, and Bihan Wen. 2023. Shadowdiffusion: When degradation prior meets diffusion model for shadow removal. In *Proceedings of the IEEE/CVF Conference on Computer Vision and Pattern Recognition*. 14049–14058.
- [15] Yu Guo, Yuan Gao, Yuxu Lu, Ryan Wen Liu, and Shengfeng He. 2024. OneRestore: A Universal Restoration Framework for Composite Degradation. In *European Conference on Computer Vision*.
- [16] Kaiming He, Jian Sun, and Xiaoou Tang. 2010. Single Image Haze Removal Using Dark Channel Prior. *IEEE Transactions on Pattern Analysis and Machine Intelligence* 33, 12 (2010), 2341–2353.
- [17] Jonathan Ho, Ajay Jain, and Pieter Abbeel. 2020. Denoising Diffusion Probabilistic Models. *Advances in Neural Information Processing Systems (NeurIPS)* 33 (2020), 6840–6851. 2020.
- [18] Phillip Isola, Jun-Yan Zhu, Tinghui Zhou, and Alexei A. Efros. 2017. Image-to-image translation with conditional adversarial networks. In *Proceedings of the IEEE Conference on Computer Vision and Pattern Recognition*. 1125–1134.
- [19] Priyank Jaini, Andre Fu, Max Z Chen, and Didrik Nielsen. 2024. Multi-Flow VAE: Continuous Normalizing Flows for VAEs Revisited. In *The Twelfth International Conference on Learning Representations (ICLR)*.
- [20] Kui Jiang, Zhongyuan Wang, Peng Yi, Chen Chen, Zheng Wang, Xiao Wang, Junjun Jiang, and Chia-Wen Lin. 2021. Rain-free and residue hand-in-hand: A progressive coupled network for real-time image deraining. *IEEE Transactions on Image Processing* 30 (2021), 7404–7418.
- [21] Yeyang Jin, Wei Ye, Wenhan Yang, Yuan Yuan, and Robby T Tan. 2024. Des3: Adaptive attention-driven self and soft shadow removal using vit similarity. In *Proceedings of the AAAI Conference on Artificial Intelligence*. 2634–2642.
- [22] Junjie Ke, Qifei Wang, Yilin Wang, Peyman Milanfar, and Feng Yang. 2021. MUSIQ: Multi-scale image quality transformer. In *Proceedings of the IEEE/CVF International Conference on Computer Vision*. 5148–5157.
- [23] Boyun Li, Xiao Liu, Peng Hu, Zhongqin Wu, Jiancheng Lv, and Xi Peng. 2022. All-In-One Image Restoration for Unknown Corruption. In *IEEE Conference on Computer Vision and Pattern Recognition*. New Orleans, LA.
- [24] Haoying Li, Yifan Yang, Meng Chang, Shiqi Chen, Huajun Feng, Zhihai Xu, Qi Li, and Yueting Chen. 2022. Srdiff: Single image super-resolution with diffusion probabilistic models. *Neurocomputing* 479 (2022), 47–59.
- [25] Ruoteng Li, Loong-Fah Cheong, and Robby T. Tan. 2019. Heavy rain image restoration: Integrating physics model and conditional adversarial learning. In *Proceedings of the IEEE/CVF Conference on Computer Vision and Pattern Recognition (CVPR)*.
- [26] Ruoteng Li, Robby T. Tan, and Loong-Fah Cheong. 2020. All in One Bad Weather Removal Using Architectural Search. In *Proceedings of the IEEE/CVF Conference on Computer Vision and Pattern Recognition (CVPR)*. 3175–3185.
- [27] Xia Li, Jianlong Wu, Zhouchen Lin, Hong Liu, and Hongbin Zha. 2018. Recurrent squeeze-and-excitation context aggregation net for single image deraining. In *Proceedings of the European Conference on Computer Vision (ECCV)*. 254–269.
- [28] Xing Liu, Masanori Suganuma, Zhun Sun, and Takayuki Okatani. 2019. Dual residual networks leveraging the potential of paired operations for image restoration. In *Proceedings of the IEEE/CVF Conference on Computer Vision and Pattern Recognition*. 7007–7016.
- [29] Yun-Fu Liu, Da-Wei Jaw, Shih-Chia Huang, and Jenq-Neng Hwang. 2018. Desdownet: Context-aware deep network for snow removal. *IEEE Transactions on Image Processing* 27, 6 (2018), 3064–3073.
- [30] Anish Mittal, Anush Krishna Moorthy, and Alan Conrad Bovik. 2012. No-reference image quality assessment in the spatial domain. *IEEE TIP* 21, 12 (2012), 4695–4708.
- [31] Chong Mou, Qian Wang, and Jian Zhang. 2022. Deep Generalized Unfolding Networks for Image Restoration. In *CVPR*.
- [32] Ozan Özdenizci and Robert Legenstein. 2023. Restoring Vision in Adverse Weather Conditions with Patch-Based Denoising Diffusion Models. *IEEE Transactions on Pattern Analysis and Machine Intelligence (TPAMI)* (2023).

- [33] Ozan Özdenizci and Robert Legenstein. 2023. Restoring vision in adverse weather conditions with patch-based denoising diffusion models. *IEEE Transactions on Pattern Analysis and Machine Intelligence* (2023), 1–12. <https://doi.org/10.1109/TPAMI.2023.3238179>
- [34] Vaishnav Potlapalli, Syed Waqas Zamir, Salman Khan, and Fahad Khan. 2023. PromptIR: Prompting for All-in-One Image Restoration. In *Thirty-seventh Conference on Neural Information Processing Systems*.
- [35] Rui Qian, Robby T Tan, Wenhan Yang, Jiajun Su, and Jiaying Liu. 2018. Attentive generative adversarial network for raindrop removal from a single image. In *Proceedings of the IEEE conference on computer vision and pattern recognition*. 2482–2491.
- [36] Ruijie Quan, Xin Yu, Yuanzhi Liang, and Yi Yang. 2021. Removing raindrops and rain streaks in one go. In *Proceedings of the IEEE/CVF Conference on Computer Vision and Pattern Recognition*. 9147–9156.
- [37] Yuhui Quan, Shijie Deng, Yixin Chen, and Hui Ji. 2019. Deep learning for seeing through window with raindrops. In *Proceedings of the IEEE/CVF International Conference on Computer Vision*. 2463–2471.
- [38] Chitwan Saharia, Jonathan Ho, William Chan, Tim Salimans, David J Fleet, and Mohammad Norouzi. 2022. Image super-resolution via iterative refinement. *IEEE Transactions on Pattern Analysis and Machine Intelligence* 45, 4 (2022), 4713–4726.
- [39] Binbin Song, Xiangyu Chen, Shuning Xu, and Jiantao Zhou. 2023. Under-display camera image restoration with scattering effect. In *Proceedings of the IEEE/CVF International Conference on Computer Vision*. 12580–12589.
- [40] Yuda Song, Zhuqing He, Hui Qian, and Xin Yu. 2023. DehazeFormer: Vision Transformer-Based Architecture for Single Image Dehazing. In *Proceedings of the IEEE/CVF Conference on Computer Vision and Pattern Recognition (CVPR)*. 12345–12354.
- [41] Shaolin Su, Qingsen Yan, Yu Zhu, Cheng Zhang, Xin Ge, Jinqiu Sun, and Yanning Zhang. 2020. Blindly assess image quality in the wild guided by a self-adaptive hyper network. *Proceedings of the IEEE/CVF Conference on Computer Vision and Pattern Recognition*, 3667–3676.
- [42] Jeya Maria Jose Valanarasu, Rajeev Yasarla, and Vishal M Patel. 2022. Transweather: Transformer-based restoration of images degraded by adverse weather conditions. In *Proceedings of the IEEE/CVF Conference on Computer Vision and Pattern Recognition*. 2353–2363.
- [43] Jianyi Wang, Zongsheng Yue, Shangchen Zhou, Kelvin C. K. Chan, and Chen Change Loy. 2023. Exploiting Diffusion Prior for Real-World Image Super-Resolution. In *Proceedings of the IEEE/CVF International Conference on Computer Vision (ICCV)*. 12345–12354.
- [44] Tianyu Wang, Xin Yang, Ke Xu, Shaozhe Chen, Qiang Zhang, and Rynson WH Lau. 2019. Spatial attentive single-image deraining with a high quality real rain dataset. In *Proceedings of the IEEE/CVF conference on computer vision and pattern recognition*. 12270–12279.
- [45] Xinlong Wang, Wen Wang, Yue Cao, Chunhua Shen, and Tiejun Huang. 2023. Images speak in images: A generalist painter for in-context visual learning. In *Proceedings of the IEEE/CVF Conference on Computer Vision and Pattern Recognition*. 6830–6839.
- [46] Zhou Wang, Alan C Bovik, Hamid R Sheikh, and Eero P Simoncelli. 2004. Image quality assessment: from error visibility to structural similarity. *IEEE TIP* 13, 4 (2004), 600–612.
- [47] Haoning Wu, Zicheng Zhang, Erli Zhang, Chaofeng Chen, Liang Liao, Annan Wang, Li Chunyi, Wenxiu Sun, Qiong Yan, Guangtao Zhai, et al. 2024. Q-Bench: A benchmark for general-purpose foundation models on low-level vision. In *ICLR* (2024).
- [48] Haoning Wu, Zicheng Zhang, Erli Zhang, Chaofeng Chen, Liang Liao, Annan Wang, Kaixin Xu, Chunyi Li, Jingwen Hou, Guangtao Zhai, et al. 2024. Q-Instruct: Improving low-level visual abilities for multi-modality foundation models. In *Proceedings of the IEEE/CVF Conference on Computer Vision and Pattern Recognition*.
- [49] Haoning Wu, Zicheng Zhang, Weixia Zhang, Chaofeng Chen, Chunyi Li, Liang Liao, Annan Wang, Erli Zhang, Wenxiu Sun, Qiong Yan, Xiongkuo Min, Guangtai Zhai, and Weisi Lin. 2023. Q-Align: Teaching LLMs for Visual Scoring via Discrete Text-Defined Levels. *arXiv preprint arXiv:2312.17090* (2023). Equal Contribution by Wu, Haoning and Zhang, Zicheng. Project Lead by Wu, Haoning. Corresponding Authors: Zhai, Guangtai and Lin, Weisi.
- [50] Haoning Wu, Zicheng Zhang, Weixia Zhang, Chaofeng Chen, Liang Liao, Chunyi Li, Yixuan Gao, Annan Wang, Erli Zhang, Wenxiu Sun, et al. 2024. Q-Align: Teaching LLMs for visual scoring via discrete text-defined levels. In *ICML*.
- [51] Jie Xiao, Xueyang Fu, Aiping Liu, Feng Wu, and Zheng-Jun Zha. 2022. Image de-raining transformer. *IEEE Transactions on Pattern Analysis and Machine Intelligence* (2022).
- [52] Zhenhua Xu, Yujia Zhang, Enze Xie, Zhen Zhao, Yong Guo, Kwan-Yee K Wong, Zhenguo Li, and Hengshuang Zhao. 2024. Drivegpt4: Interpretable end-to-end autonomous driving via large language model. *IEEE Robotics and Automation Letters* (2024).
- [53] Tao Yang, Peiran Ren, Xuansong Xie, and Lei Zhang. 2023. Pixel-aware stable diffusion for realistic image super-resolution and personalized stylization. *arXiv preprint arXiv:2308.14469* (2023).
- [54] Wenhan Yang, Robby T. Tan, Jiashi Feng, Jiaying Liu, Zongming Guo, and Shuicheng Yan. 2017. Deep Joint Rain Detection and Removal from a Single Image. In *Proceedings of the IEEE Conference on Computer Vision and Pattern Recognition (CVPR)*. 1357–1366.
- [55] Tian Ye, Sixiang Chen, Jinbin Bai, Jun Shi, Chenghao Xue, Jingxia Jiang, Junjie Yin, Erkang Chen, and Yun Liu. 2023. Adverse weather removal with codebook priors. In *Proceedings of the IEEE/CVF International Conference on Computer Vision*. 12653–12664.
- [56] Zhiyuan You, Xin Cai, Jinjin Gu, Tianfan Xue, and Chao Dong. 2025. Teaching Large Language Models to Regress Accurate Image Quality Scores using Score Distribution. In *IEEE Conference on Computer Vision and Pattern Recognition*.
- [57] Syed Waqas Zamir, Aditya Arora, Salman Khan, Munawar Hayat, Fahad Shahbaz Khan, and Ming-Hsuan Yang. 2022. Restormer: Efficient Transformer for High-Resolution Image Restoration. In *CVPR*.
- [58] Syed Waqas Zamir, Aditya Arora, Salman Khan, Munawar Hayat, Fahad Shahbaz Khan, Ming-Hsuan Yang, and Ling Shao. 2021. Multi-Stage Progressive Image Restoration. In *CVPR*.
- [59] Syed Waqas Zamir, Aditya Arora, Salman Khan, Munawar Hayat, Fahad Shahbaz Khan, Ming-Hsuan Yang, and Ling Shao. 2021. Multi-stage progressive image restoration. In *Proceedings of the IEEE/CVF Conference on Computer Vision and Pattern Recognition*. 14821–14831.
- [60] Kaihao Zhang, Rongqing Li, Yanjiang Yu, Wenhan Luo, and Changsheng Li. 2021. Deep Dense Multi-scale Network for Snow Removal Using Semantic and Geometric Priors. *IEEE Transactions on Image Processing* (2021).
- [61] Richard Zhang, Phillip Isola, Alexei A Efros, Eli Shechtman, and Oliver Wang. 2018. The unreasonable effectiveness of deep features as a perceptual metric. *Proceedings of the IEEE conference on computer vision and pattern recognition* (2018), 586–595.
- [62] Man Zhou, Jie Huang, Chun-Le Guo, and Chongyi Li. 2023. Fourmer: An efficient global modeling paradigm for image restoration. In *International conference on machine learning*. PMLR, 42589–42601.
- [63] Xiaoyu Zhou, Zhiwei Lin, Xiaojun Shan, Yongtao Wang, Deqing Sun, and Ming-Hsuan Yang. 2024. Drivingsplatt: Composite gaussian splatting for surrounding dynamic autonomous driving scenes. In *Proceedings of the IEEE/CVF Conference on Computer Vision and Pattern Recognition*. 21634–21643.
- [64] Hanwei Zhu, Haoning Wu, Yixuan Li, Zicheng Zhang, Baoliang Chen, Lingyu Zhu, Yuming Fang, Guangtao Zhai, Weisi Lin, and Shiqi Wang. 2024. Adaptive Image Quality Assessment via Teaching Large Multimodal Model to Compare. *arXiv preprint arXiv:2405.19298* (2024).
- [65] Jun-Yan Zhu, Taesung Park, Phillip Isola, and Alexei A. Efros. 2017. Unpaired Image-to-Image Translation Using Cycle-Consistent Adversarial Networks. In *Proceedings of the IEEE International Conference on Computer Vision (ICCV)*. 2223–2232.
- [66] Yurui Zhu, Tianyu Wang, Xueyang Fu, Xuanyu Yang, Xin Guo, Jifeng Dai, Yu Qiao, and Xiaowei Hu. 2023. Learning Weather-General and Weather-Specific Features for Image Restoration Under Multiple Adverse Weather Conditions. In *Proc. IEEE/CVF Conference on Computer Vision and Pattern Recognition (CVPR)*.

A OVERVIEW

This supplementary material provides extended details on our AdaQual-Diff framework, comprehensive experimental validation, and additional analysis not included in the main paper due to space constraints. The supplementary content is organized as follows:

- Section B: Detailed information about dataset configurations.
- Section C: Architecture of the AdaQual-Diff framework.
- Section D: Additional Qualitative Results.
- Section E: Ablation Study
- Section F: Limitation discussion.
- Section G: Future works.

B DATASET CONFIGURATIONS

Composite Degradation Dataset. To evaluate the model’s capability in handling multiple simultaneous degradations, we adopt the publicly available CDD-11 dataset [15]. This dataset contains 13,013 degraded/clear image pairs for training and 2,200 pairs reserved for testing. It encompasses 11 distinct degradation categories: low-light, haze, rain, snow, and their various combinations (low+haze, low+rain, low+snow, haze+rain, haze+snow, low+haze+rain, and low+haze+snow).

Adverse Weather Benchmark Datasets. Following previous work [6], we evaluate our proposed method on several established benchmark datasets targeting specific adverse weather conditions. **Snow100K [29]:** Designed for image snow removal, this dataset includes testing subsets Snow100K-S, Snow100K-M, and Snow100K-L (representing light, medium, and heavy synthetic snow) and Snow100K-Real (real-world snowy images). We utilize these subsets for evaluation.

Outdoor-Rain [25]: This benchmark focuses on the removal of both rain and haze. For quantitative analysis, we employ the Test1 subset, which contains 750 high-definition images characterized by dense rain and realistic haze.

RainDrop [35]: Featuring images with simulated raindrops on the camera lens, we evaluate our method using the RainDrop-A test subset consisting of 58 images.

C ADAQUAL-DIFF ARCHITECTURE

Regarding the diffusion process architecture, AdaQualDiff introduces a distinct and arguably more direct paradigm for adaptive restoration compared to methods like T^3 -DiffWeather. While T^3 -DiffWeather innovatively utilizes a prompt pool to dynamically construct *weather-specific prompts* based on degradation residuals and employs *depth features* for general scene guidance, AdaQualDiff pioneers a strategy fundamentally rooted in *direct perceptual quality assessment*. Our core creative contribution, the Adaptive Quality Prompting mechanism, moves beyond selecting from predefined pools based on indirect features. Instead, it establishes a direct mathematical relationship between *local image quality scores* (quantified by DeQAScore) and the required *structural complexity and computational intensity* of the guidance prompt itself ($C_p \propto f(1 - Q)$). This contrasts significantly with T^3 -DiffWeather’s approach, which relies on learned correlations between sub-prompts, degradation types, and scene features. AdaQualDiff’s ingenuity lies in its ability to generate a *spatially-varying guidance field* where restoration effort is precisely and dynamically allocated based solely on the

measured quality deficit in each region. This allows for exceptionally fine-grained control over the restoration process, directly addressing the severity of degradation without explicit decomposition into weather types or reliance on auxiliary scene representations like depth maps. This quality-driven adaptivity allows our framework to achieve state-of-the-art results with potentially comparable or fewer parameters.

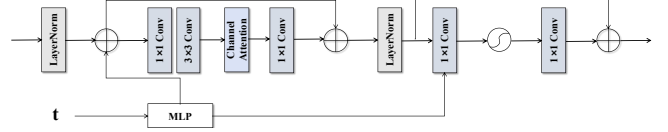


Figure 8: Structure of the NAFNet Block.

D ADDITIONAL QUALITATIVE RESULTS

D.1 More Results on CDD-11 Dataset

We provide additional visual comparisons on the CDD-11 dataset to demonstrate the effectiveness of AdaQual-Diff in handling complex composite degradations. Figures 9 and 10 (adjust figure references as needed) showcase the results. As observed, AdaQual-Diff achieves superior restoration, producing results closer to the ground truth images compared to existing methods, particularly in recovering fine details and accurate colors under various combined degradations.

D.2 More Results on Classic Benchmarks

We further present extended qualitative results on established benchmark datasets, including Snow100K, Outdoor-Rain, and RainDrop. Figures 12 illustrates these comparisons. The figures highlight AdaQual-Diff’s ability to generate visually pleasing results that significantly surpass previous methods in terms of overall image detail, texture preservation, and color fidelity across different adverse weather conditions (snow, rain, haze) and raindrop scenarios.

E ABLATION STUDY

In this section, we specifically analyze the sensitivity of the AdaQual-Diff framework to the quality threshold parameter, τ . This threshold is a crucial element within our Adaptive Quality Prompting mechanism. It determines how the intensity and nature of the restoration guidance (provided via prompts) are modulated based on the input image’s perceived quality score Q . This score Q itself can be informed by advanced assessment methods like DeQA-Score, which notably considers the distribution (mean and variance) of quality scores rather than just a single mean value, highlighting the inherent uncertainty in quality perception.

F LIMITATIONS

Despite the compelling results generated by our proposed pipeline, it also faces some inherent limitations. Firstly, a core characteristic of diffusion models is the significant computational resources required for both training and the iterative inference process. This factor, combined with the model’s relatively large parameter count compared to traditional regression methods or other generative

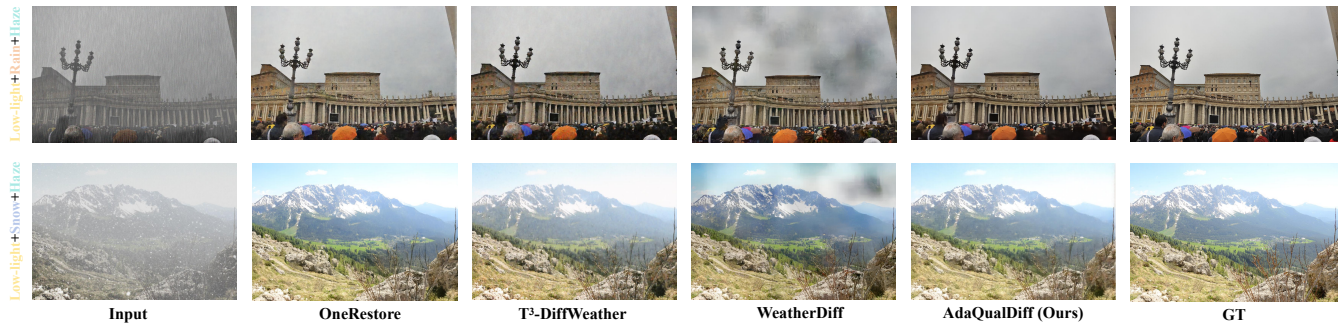


Figure 9: Qualitative comparison on the CDD-11 dataset.



Figure 10: Qualitative comparison on the CDD-11 dataset.

Table 8: Ablation study examining the effect of the quality threshold τ on the restoration performance on the CDD-11 dataset.

Threshold τ	PSNR \uparrow	SSIM \uparrow
1.5 (Low Threshold)	28.91	0.878
3.0 (Selected)	30.11	0.900
4.5 (High Threshold)	29.75	0.875

frameworks (e.g., VAEs [11, 19]), potentially hinders deployment in resource-constrained or real-time scenarios.

G FUTURE WORK

Looking ahead, several avenues warrant further investigation. A key priority is to explore methods for reducing the parameter count of our model, potentially through model compression techniques or architectural refinements, without compromising performance. We

also aim to further refine the core mechanisms presented herein, enhancing their effectiveness and robustness. Extending the applicability of our pipeline to encompass a wider range of image restoration tasks within a unified "all-in-one" framework represents a significant future goal. Concurrently, we will continue to scrutinize the pipeline design to eliminate any potential redundancies and optimize overall efficiency.

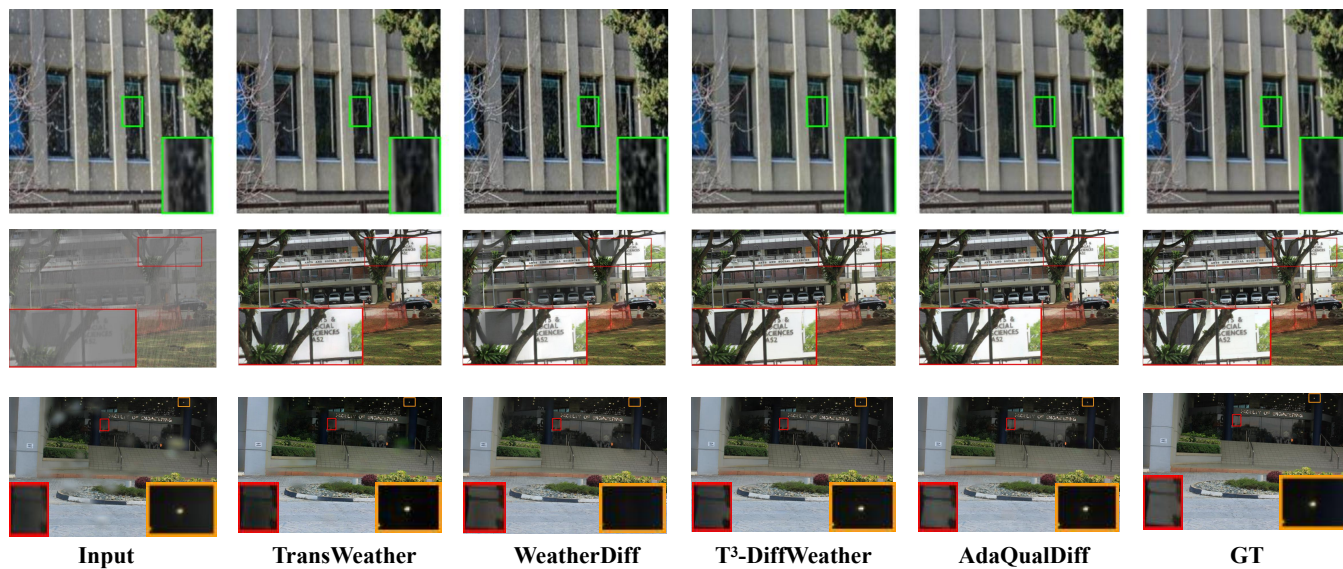


Figure 11: Qualitative comparisons on benchmark datasets Snow100K, Outdoor-Rain, and RainDrop.

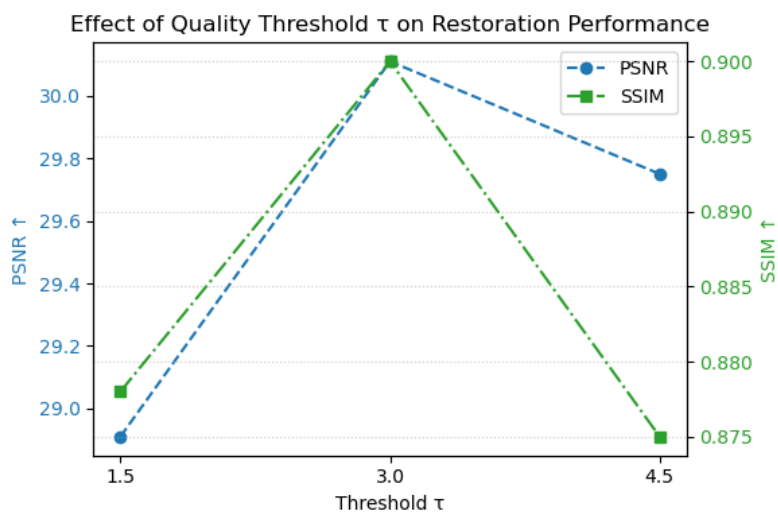


Figure 12: Abl. of the quality threshold τ .